Available online at www.sciencedirect.com
SCIENCE DIRECT®
Journal of Sound and Vibration 279 (2005) 389–402
JOURNAL OF SOUND AND VIBRATION
www.elsevier.com/locate/jsvi

Reproducing kernel particle method for free and forced vibration analysis ☆

J.X. Zhou*, H.Y. Zhang, L. Zhang

School of Civil Engineering and Mechanics, Xi'an Jiaotong University, Xi'an 710049, PR China

Received 10 March 2003; accepted 7 November 2003

Abstract

A reproducing kernel particle method (RKPM) is presented to analyze the natural frequencies of Euler–Bernoulli beams as well as Kirchhoff plates. In addition, RKPM is also used to predict the forced vibration responses of buried pipelines due to longitudinal travelling waves. Two different approaches, Lagrange multipliers as well as transformation method , are employed to enforce essential boundary conditions. Based on the reproducing kernel approximation, the domain of interest is discretized by a set of particles without the employment of a structured mesh, which constitutes an advantage over the finite element method. Meanwhile, RKPM also exhibits advantages over the classical Rayleigh–Ritz method and its counterparts. Numerical results presented here demonstrate the effectiveness of this novel approach for both free and forced vibration analysis.

1. Introduction

For distributed parameter systems, the dynamic models for free and forced vibration are governed by a group of partial differential equations as well as a set of boundary conditions. Close-form solutions to these problems are possible only in relatively few cases, recourse, therefore, must be had to numerical approaches. For this reason, numerical techniques with different discretization schemes for distributed parameter systems (beams, plates, shells, etc.) have been developed, such as the Rayleigh–Ritz method, the weighted residuals method, the finite element method (FEM), etc. Rayleigh–Ritz method and its counterparts are restricted to domain with simple geometry and to simple loading conditions, while in the FEM mesh is required and the preparation of data is arduous and time-consuming.

☆The project is supported by National Natural Science Foundation of China under Grant Number 10202018.
*Corresponding author.
E-mail address: jxzhouxx@mail.xjtu.edu.cn (J.X. Zhou).

0022-460X/$ - see front matter © 2003 Elsevier Ltd. All rights reserved.
doi:10.1016/j.jsv.2003.11.003

In recent years, a new type of numerical method called meshless or mesh-free method has been developed in the realm of computational mechanics. Among various versions of meshless methods, the element free galerkin (EFG) method and the reproducing kernel particle method (RKPM) are two well-developed techniques [1]. For RKPM, which shares the common features of all meshless methods, there is no need for explicit mesh, so mesh creation time is saved. Furthermore, there are some unique features of RKPM, such as time or space localization, hp-like adaptivity as well as multiresolution analysis. All these make RKPM a novel approach for structural dynamics, large deformation problems, computational fluid mechanics and other application areas [2–8].

Liu et al. [3] proposed RKPM for structural dynamics analysis for the first time. Dynamic large deformation analyses of 1-D and 2-D non-linear structures are performed using RKPM. Numerical results show that RKPM provides better stability than smooth particle hydrodynamics (SPH) method and allows larger time steps than the critical time step for standard FEM. Aluru [9] used RKPM to analyze static and dynamic deformation of microelectromechanical systems (MEMS). RKPM is shown to be accurate by comparing the computed peak deflections with experimental data.

Ouatouati [10] used EFG method to calculate natural frequencies and modes of beams and plates for the first time. Liu [11] also used EFG method to investigate static and free vibration analyses of plates with complicated shape. Both of them adopt moving least-squares (MLS) interpolation to construct shape functions. The reproducing kernel (RK) approximation is, alternatively, used herein to form shape functions. The resulting RKPM method is proposed to calculate natural frequencies of beams and plates with various boundary conditions such as free, simply supported and fully clamped. Furthermore, longitudinal seismic responses of buried pipelines subjected to travelling sinusoidal wave are investigated.

2. Overview of RKPM

2.1. Reproducing kernel approximation

The kernel approximation of a function $u(x)$ is written as

$$u^a(x) = \int_\Omega w_d(x-s)u(s)\,\mathrm{d}s, \tag{1}$$

where $w_d(x-s)$ is the kernel function with a dilation parameter, d, and $u^a(x)$ is the kernel approximation of $u(x)$. Liu et al. [2,3] proposed the RK approximation by introducing a correction function to the kernel approximation, which gives

$$u^a(x) = \int_\Omega \bar{w}_d(x-s)u(s)\,\mathrm{d}s, \tag{2}$$

where $\bar{w}_d(x-s) = C(x,s)w_d(x-s)$ is the corrected reproducing kernel function. $C(x,s)$ is the correction function and is expressed as a linear combination of polynomial basis functions

$$C(x,s) = c_0(x) + c_1(x)(x-s) + c_2(x-s)^2 + \cdots + c_N(x)(x-s)^N, \tag{3}$$

where $c_0(x), c_1(x), c_2(x), \ldots, c_N(x)$ are functions of x which are to be determined by the reproducing conditions. N is the highest derivatives of the governing differential equations.

Defining the moments of kernel function and corrected kernel function, respectively, in the following form:

$$m_k(x) = \int_\Omega (x-s)^k w_d(x-s)\,\mathrm{d}s, \quad k = 0, 1, 2, \ldots, \tag{4}$$

$$\bar{m}_k(x) = \int_\Omega (x-s)^k \bar{w}_d(x-s)\,\mathrm{d}s, \quad k = 0, 1, 2, \ldots, \tag{5}$$

the reproducing conditions for $u^a(x) = u(x)$ can be obtained from Eq. (4) and the Taylor series expansion of $u(s)$, and can be expressed as the following vector form:

$$\bar{\mathbf{M}} = \{\bar{m}_0(x), \bar{m}_1(x), \ldots, \bar{m}_N(x)\}^{\mathrm{T}} = \{1, 0, \ldots, 0\}^{\mathrm{T}}. \tag{6}$$

Designating $\bar{\mathbf{C}} = \{c_0(x), c_1(x), \ldots, c_N(x)\}^{\mathrm{T}}$ the unknown vector consisting of $N+1$ correction function coefficients, the unknown vector can be determined through solving the following equations:

$$\mathbf{M}\bar{\mathbf{C}} = \bar{\mathbf{M}}, \tag{7}$$

where

$$\mathbf{M} = \begin{bmatrix} m_0(x) & m_1(x) & \cdots & m_N(x) \\ m_1(x) & m_2(x) & \cdots & m_{N+1}(x) \\ \cdots & \cdots & & \cdots \\ m_N(x) & m_{N+1}(x) & \cdots & m_{2N}(x) \end{bmatrix}. \tag{8}$$

2.2. Reproducing conditions for the first derivative

Reproducing conditions for the first derivative of an approximated function can be derived in a similar fashion as described above. The reproducing conditions for $\mathrm{d}u^a(x)/\mathrm{d}x = \mathrm{d}u(x)/\mathrm{d}x$ can be written in a similar form as Eq. (6)

$$\bar{\mathbf{M}}' = \{\bar{m}'_0(x), \bar{m}'_1(x), \ldots, \bar{m}'_N(x)\}^{\mathrm{T}} = \{0, -1, 0 \ldots, 0\}^{\mathrm{T}} \tag{9}$$

in which

$$\bar{m}'_k(x) = \int_\Omega (x-s)^k \frac{\mathrm{d}}{\mathrm{d}s}[\bar{w}_d(x-s)]\,\mathrm{d}s, \quad k = 0, 1, 2, \ldots\ . \tag{10}$$

Denoting $\bar{\mathbf{C}}' = \{c'_0(x), c'_1(x), \ldots, c'_N(x)\}^{\mathrm{T}}$ the column vector comprising the gradients of the correction function coefficients, the vector can, combining Eq. (7) together, be obtained from the following equations:

$$[\mathbf{M}' \quad \mathbf{M}] \begin{bmatrix} \bar{\mathbf{C}} \\ \bar{\mathbf{C}}' \end{bmatrix} = [\mathbf{0}], \tag{11}$$

where $\mathbf{M}$ is as defined in Eq. (8), and $\mathbf{M}'$ is defined as

$$\mathbf{M}' = \begin{bmatrix} m'_0(x) & m'_1(x) & \cdots & m'_N(x) \\ m'_1(x) & m'_2(x) & \cdots & m'_{N+1}(x) \\ \cdots & \cdots & & \cdots \\ m'_N(x) & m'_{N+1}(x) & \cdots & m'_{2N}(x) \end{bmatrix}.$$

2.3. RKPM

The discretized form of reproducing kernel approximation, which is referred to as the RKPM, can be obtained by applying the trapezoidal ruler to Eq. (2) and approximating the unknown variable in the following form of RKPM shape functions:

$$u^a(x) = \sum_{I=1}^{NP} N_I(x) u_I, \tag{12}$$

where $N_I(x) = C(x, x_I) w_d(x - x_I) \Delta V_I$ is defined as the RKPM shape function for particle I , u_I is the parameter associated with particle I , ΔV_I is the influence domain of particle I , and NP is the total particle number to discretize the problem domain. For multi-dimensional problems, Eq. (12) can be written in the form of position vector $\mathbf{x}$ as follows:

$$u^a(\mathbf{x}) = \sum_{I=1}^{NP} N_I(\mathbf{x}) u_I. \tag{13}$$

3. RKPM for free vibration analysis of beams and plates

3.1. Free vibration analysis of Euler–Bernoulli beam using RKPM

The governing equation of free vibration of Euler–Bernoulli is posed as

$$\frac{\partial^2 u}{\partial t^2} + \frac{EI}{\rho A} \frac{\partial^4 u}{\partial x^4} = 0, \tag{14}$$

where u is the displacement, and E and ρ are, respectively, the Young's modulus and mass density of the material, and I and A are, respectively, the moment of inertia and area of cross-sections.

Without loss of generality, the clamped–simply supported beam is chosen as an example for the purpose of illustration. Applying virtual work principle and using Lagrange multipliers to impose the corresponding boundary conditions lead to the following statement:

$$\delta \bar{\Pi} = \int_x \frac{\partial^2 u}{\partial x^2} \frac{\partial^2 \delta u}{\partial x^2} \mathrm{d}x + \frac{\rho A}{EI} \int_x \frac{\partial^2 u}{\partial t^2} \delta u \, \mathrm{d}x + \lambda_1 \delta u|_0^l + \delta \lambda_1 u|_0^l + \lambda_2 \delta \left. \frac{\partial u}{\partial x} \right|_0 + \delta \lambda_2 \left. \frac{\partial u}{\partial x} \right|_0 = 0, \tag{15}$$

where l is the total length of beam, λ_1 and λ_2 are two Lagrange multipliers, respectively.

In order to identify the meanings of Lagrange multipliers λ_1 and λ_2, Eq. (15) can be manipulated as follows:

$$\delta\bar{\Pi} = \int_x \frac{\partial^4 u}{\partial x^4}\delta u\,\mathrm{d}x + \frac{\rho A}{EI}\int_x \frac{\partial^2 u}{\partial t^2}\delta u\,\mathrm{d}x + \frac{\partial^2 u}{\partial x^2}\delta\frac{\partial u}{\partial x}\bigg|_l + \left(\lambda_2 - \frac{\partial^2 u}{\partial x^2}\right)\delta\frac{\partial u}{\partial x}\bigg|_0 + \left(\lambda_1 - \frac{\partial^3 u}{\partial x^3}\right)\delta u\big|_0^l + \delta\lambda_1 u\big|_0^l + \delta\lambda_2\frac{\partial u}{\partial x}\bigg|_0 = 0. \tag{16}$$

The identification of λ_1 and λ_2 is, therefore, readily obtained as follows:

$$\lambda_1 = \frac{\partial^3 u}{\partial x^3}, \quad \lambda_2 = \frac{\partial^2 u}{\partial x^2}. \tag{17}$$

Substituting λ_1 and λ_2 given above into Eq. (15) gives

$$\int_x \frac{\partial^2 u}{\partial x^2}\frac{\partial^2 \delta u}{\partial x^2}\,\mathrm{d}x + \frac{\rho A}{EI}\int_x \frac{\partial^2 u}{\partial t^2}\delta u\,\mathrm{d}x + \frac{\partial^3 u}{\partial x^3}\delta u\bigg|_0^l + \delta\frac{\partial^3 u}{\partial x^3}u\bigg|_0^l + \frac{\partial^2 u}{\partial x^2}\delta\frac{\partial u}{\partial x}\bigg|_0 + \delta\frac{\partial^2 u}{\partial x^2}\frac{\partial u}{\partial x}\bigg|_0 = 0. \tag{18}$$

Eq. (18) is the derived weak form to the strong form given in Eq. (14) with corresponding clamped–simply supported boundary conditions. Following the same procedure, the weak forms corresponding to other boundary conditions can be summarized as follows:

(a) *Simply supported–simply supported*:

$$\int_x \frac{\partial^2 u}{\partial x^2}\frac{\partial^2 \delta u}{\partial x^2}\,\mathrm{d}x + \frac{\rho A}{EI}\int_x \frac{\partial^2 u}{\partial t^2}\delta u\,\mathrm{d}x + \frac{\partial^3 u}{\partial x^3}\delta u\bigg|_0^l + \delta\frac{\partial^3 u}{\partial x^3}u\bigg|_0^l = 0. \tag{19}$$

(b) *Clamped–free*:

$$\int_x \frac{\partial^2 u}{\partial x^2}\frac{\partial^2 \delta u}{\partial x^2}\,\mathrm{d}x + \frac{\rho A}{EI}\int_x \frac{\partial^2 u}{\partial t^2}\delta u\,\mathrm{d}x - \frac{\partial^3 u}{\partial x^3}\delta u\bigg|_0 - \delta\frac{\partial^3 u}{\partial x^3}u\bigg|_0 + \frac{\partial^2 u}{\partial x^2}\delta\frac{\partial u}{\partial x}\bigg|_0 + \delta\frac{\partial^2 u}{\partial x^2}\frac{\partial u}{\partial x}\bigg|_0 = 0. \tag{20}$$

(c) *Clamped–clamped*:

$$\int_x \frac{\partial^2 u}{\partial x^2}\frac{\partial^2 \delta u}{\partial x^2}\,\mathrm{d}x + \frac{\rho A}{EI}\int_x \frac{\partial^2 u}{\partial t^2}\delta u\,\mathrm{d}x + \frac{\partial^3 u}{\partial x^3}\delta u\bigg|_0^l + \delta\frac{\partial^3 u}{\partial x^3}u\bigg|_0^l - \frac{\partial^2 u}{\partial x^2}\delta\frac{\partial u}{\partial x}\bigg|_0^l - \delta\frac{\partial^2 u}{\partial x^2}\frac{\partial u}{\partial x}\bigg|_0^l = 0. \tag{21}$$

With the weak forms given in Eq. (19)–(21) at hand, RKPM discretization procedure can now be used to obtain the discretized equations. As an example, only Eq. (21) corresponding to clamped–clamped boundary conditions is discretized by RKPM and the resulting stiffness and mass matrices are given herein, and other equations can be treated in a similar manner.

Expressing u and δu in the form of Eq. (12), i.e.,

$$u = \sum_{B=1}^{NP} N_B u_B = \mathbf{Nu}, \tag{22}$$

$$\delta u = \sum_{A=1}^{NP} N_A v_A = \mathbf{Nv} \tag{23}$$

and substituting Eqs. (22) and (23) into Eq. (21), the resulting stiffness and mass matrices can be written in the following expressions:

$$\mathbf{M} = \int_x \frac{\rho A}{EI} \mathbf{N}^{\mathrm{t}} \mathbf{N} \, \mathrm{d}x, \tag{24}$$

$$\mathbf{K} = \int_x \frac{\partial^2 \mathbf{N}}{\partial x^2} \frac{\partial^2 \mathbf{N}^{\mathrm{t}}}{\partial x^2} \, \mathrm{d}x + \frac{\partial^3 \mathbf{N}}{\partial x^3} \mathbf{N}^{\mathrm{t}} \Big|_0^l + \mathbf{N} \frac{\partial^3 \mathbf{N}^{\mathrm{t}}}{\partial x^3} \Big|_0^l - \frac{\partial^2 \mathbf{N}}{\partial x^2} \frac{\partial \mathbf{N}^{\mathrm{t}}}{\partial x} \Big|_0^l - \frac{\partial \mathbf{N}}{\partial x} \frac{\partial^2 \mathbf{N}^{\mathrm{t}}}{\partial x^2} \Big|_0^l. \tag{25}$$

3.2. Free vibration analysis of Kirchhoff plate using RKPM

Following the similar procedures for deriving weak forms of free vibration beams, the weak form of Kirchhoff plate is derived as follows:

$$\rho \int \left(h \ddot{w} \delta w + \frac{h^3}{12} w_{,x} \, \delta w_{,x} + \frac{h^3}{12} w_{,y} \, \delta w_{,y} \right) \mathrm{d}x \, \mathrm{d}y + D \int (w_{,xx} \, \delta w_{,xx} + w_{,yy} \, \delta w_{,yy}) \, \mathrm{d}x \, \mathrm{d}y$$
$$+ \; vD \int (w_{,xx} \, \delta w_{,yy} + w_{,yy} \, \delta w_{,xx}) \, \mathrm{d}x \, \mathrm{d}y + 2D(1 - v) \int w_{,xy} \, \delta w_{,xy} \, \mathrm{d}x \, \mathrm{d}y = 0, \tag{26}$$

where w denotes displacement of plate, and v, h and D represent the Poisson ratio, the thickness of plate, the flexural stiffness of the plate, respectively.

Approximating w and δw in the form given by Eq. (12) and substituting them into Eq. (26) yield the mass and stiffness matrices in the following form:

$$\mathbf{M} = \rho \int \left[h \mathbf{N}^{\mathrm{t}}(x, y) \mathbf{N}(x, y) + \frac{h^3}{12} \frac{\partial \mathbf{N}^{\mathrm{t}}(x, y)}{\partial x} \frac{\partial \mathbf{N}(x, y)}{\partial x} + \frac{h^3}{12} \frac{\partial \mathbf{N}^{\mathrm{t}}(x, y)}{\partial y} \frac{\partial \mathbf{N}(x, y)}{\partial y} \right] \mathrm{d}x \, \mathrm{d}y, \tag{27}$$

$$\mathbf{K} = \int \left(\begin{bmatrix} \dfrac{\partial^2}{\partial x^2} \\ \dfrac{\partial^2}{\partial y^2} \\ 2 \dfrac{\partial^2}{\partial x \partial y} \end{bmatrix} \mathbf{N}^{\mathrm{t}}(x, y) \right)^{\mathrm{t}} D \begin{bmatrix} 1 & v & 0 \\ v & 1 & 0 \\ 0 & 0 & \dfrac{1 - v}{2} \end{bmatrix} \left(\begin{bmatrix} \dfrac{\partial^2}{\partial x^2} \\ \dfrac{\partial^2}{\partial y^2} \\ 2 \dfrac{\partial^2}{\partial x \partial y} \end{bmatrix} \mathbf{N}^{\mathrm{t}}(x, y) \right) \mathrm{d}x \, \mathrm{d}y. \tag{28}$$

3.3. Boundary conditions treatment by transformation method

Due to lack of Kronecker delta property in the RKPM shape functions, the essential boundary conditions need to be treated with additional efforts. The boundary conditions of Euler–Bernoulli beams are treated through a Lagrange multipliers technique. We will now use alternative the so-called transformation method to deal with the essential boundary conditions encountered in Kirchhoff plate problems. The transformation method is presented and used by Chen [5] and Aluru et al. [9].

Using the transformation method, the transformation matrix is formed by establishing the relationship between the nodal value $u(x_I) = \hat{d}_I$ and the nodal parameter u_I. Without loss of

generality, assuming that there are m constrained particles, the transformation matrix gives

$$\begin{bmatrix} \hat{d}_1 \\ \vdots \\ \hat{d}_m \\ \hat{d}_{m+1} \\ \vdots \\ \hat{d}_{NP} \end{bmatrix} = \underbrace{\begin{bmatrix} & & & & & \\ N_1(x_1) & \cdots & N_m(x_1) & N_{m+1}(x_1) & \cdots & N_{NP}(x_1) \\ \vdots & \vdots & \vdots & \vdots & \vdots & \vdots \\ N_1(x_m) & \cdots & N_m(x_m) & N_{m+1}(x_m) & \cdots & N_{NP}(x_m) \\ N_1(x_{m+1}) & \cdots & N_m(x_{m+1}) & N_{m+1}(x_{m+1}) & \cdots & N_{NP}(x_{m+1}) \\ \vdots & \vdots & \vdots & \vdots & \vdots & \vdots \\ N_1(x_{NP}) & \cdots & N_m(x_{NP}) & N_{m+1}(x_{NP}) & \cdots & N_{NP}(x_{NP}) \end{bmatrix}}_{\mathbf{T}} \begin{bmatrix} u_1 \\ \vdots \\ u_m \\ u_{m+1} \\ \vdots \\ u_{NP} \end{bmatrix}, \tag{29}$$

where $\mathbf{T}$ is the co-ordinate transformation matrix. The shape functions can also be transformed by

$$\hat{N}_I(\mathbf{x}) = \sum_{J=1}^{NP} \mathbf{T}_{JI}^{-1} N_J(\mathbf{x}) \tag{30}$$

and

$$u^a(\mathbf{x}) = \sum_{I=1}^{NP} N_I(\mathbf{x}) u_I = \sum_{I=1}^{NP} \hat{N}_I(\mathbf{x}) \hat{d}_I. \tag{31}$$

Note that the transformed shape functions now bear the Kronecker delta property, i.e., $\hat{N}_I(\mathbf{x}_J) = \delta_{IJ}$, and the essential boundary conditions can be treated in the same manner as standard FEM followed.

3.4. RKPM results of free vibration of beams and plates

For the convenience of comparison, a dimensionless so-called natural frequency parameter, $\Omega = \beta^2 l^2 = \omega l^2 \sqrt{EI/\rho A}$ for beam or $\Omega = \beta^2 a^2 = \omega a^2 \sqrt{\rho h/D}$ for square plate (a is the length of plate), is introduced. It is more instructive to use this dimensionless parameter or its square root to compare results of different methods. Here β is the eigenvalue of the corresponding boundary value problem if separation of variables is used in analytical solution.

For the purpose of illustration, a group of beam parameters $\rho A/EI = 1$ and $l = 1$ are chosen and total particle number $NP = 21$ are selected for calculation. Natural frequency parameters up to ninth order are investigated by present RKPM method, and part of the results are presented in Table 1. Both RKPM numerical results and analytical results are given and compared. Presented comparison indicates that the RKPM results are in good agreement with the analytical results for both low and high order modes results. It is also shown that, for RKPM method, the results are fairly good even for small number of particles.

Table 1
The dimensionless natural frequency parameters

Mode	Clamped–clamped beam		Simply supported–clamped beam	
	Analytical result	RKPM result	Analytical result	RKPM result
1	22.373	21.316	15.421	15.573
2	61.670	56.731	49.965	50.982
3	120.91	118.510	104.25	102.911
7	555.16	555.651	518.77	497.174
8	713.08	717.664	671.75	675.081
9	890.74	935.929	844.47	817.915

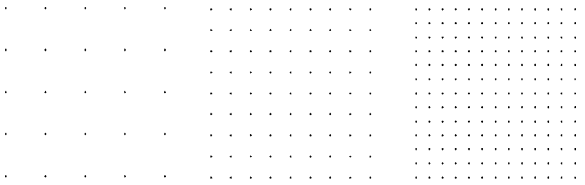

Fig. 1. Domain discretization of a square plate ((a) 5×5 nodes, (b) 9×9 nodes, and (c) 13×13 nodes).

Now consider a thin square plate with the following parameters: length $a = b = 1.0$ m; thickness $h = 0.05$ m; Young's modulus $E = 200 \times 10^9$ N/m^2: the Poission ratio $v = 0.3$; and mass density $\rho = 8000$ kg/m^3. Three different numbers of particles, i.e., 5×5, 9×9, 13×13 are used to calculate the square roots of natural frequency parameters of plate with all four sides free. The distribution of particles in the plate is shown in Figs. 1(a)–(c), respectively. In order to verify the correctness and effectiveness of RKPM, another popular meshless method, EFG method and the classic FEM are applied to solve the same problem. The results of these three numerical methodologies as well as the analytical results are presented in Table 2. For the FEM results, HOE denotes eight-noded semi-loof thin shell element (4×4 mesh); LOE denotes four-noded iso-parametric shell element (8×8 mesh) [11]. It is observed that, with regard to the square roots of dimensionless natural frequency parameters, the results obtained using RKPM are somewhere between those of FEM using HOE and LOE. Meanwhile, for majority of modes, RKPM provides improved accuracy and convergence as particles increased.

For the plate with all four sides simply supported, 13×13 particles are scattered in the domain to calculate the dimensionless natural frequency parameters. The RKPM results are also compared with the results obtained using Rayleigh–Ritz method and are given in Table 3. From Table 3, the following conclusion can be reached: there is fairly good agreement between the RKPM results and the analytical results not only for lower order modes but also for higher order modes; while for Rayleigh–Ritz method, only the results obtained for lower modes are reasonable.

Table 2
The square roots of the dimensionless natural frequency parameters

Mode	Analytical	RKPM	EFG	RKPM	EFG	RKPM	EFG	FEM [11]	
		5×5	5×5	9×9	9×9	13×13	13×13	HOE	LOE
4	3.670	3.688	3.691	3.672	3.672	3.671	3.671	3.567	3.682
5	4.427	4.431	4.433	4.433	4.434	4.430	4.430	4.423	4.466
6	4.926	4.936	4.938	4.937	4.94	4.931	4.932	4.875	4.997
7	5.929	5.942	5.934	5.908	5.911	5.904	5.904	5.851	5.942
8	5.929	5.942	5.934	5.908	5.911	5.904	5.904	5.851	5.942
9	7.848	8.081	8.046	7.846	7.843	7.834	7.836	7.82	8.079

Table 3
The dimensionless natural frequency parameters

Mode	Rayleigh–Ritz	Analytical	RKPM
1	19.739	19.739	19.744
2	49.348	49.348	49.363
3	49.348	49.348	49.363
4	78.957	78.957	79.004
5	98.711	98.696	98.583
6	98.711	98.696	98.592
14	246.909	246.740	247.170
15	247.243	246.740	247.170
16	259.886	256.609	256.168
17	276.422	256.609	256.345
22	353.406	335.566	336.560
23	371.120	365.175	366.488
24	400.466	365.175	366.488
25	407.309	394.784	397.346

4. RKPM for forced vibration analysis of buried pipelines subjected to longitudinal travelling waves

4.1. Governing equations

Letting $u(x,t)$ denote the absolute displacement as a function of the co-ordinate along the axis of the pipeline and $u_g(x,t)$ denote the ground excitation, derivation of the vibration equation of the pipe subjected to longitudinal travelling waves gives (see Ref. [12] for details)

$$\bar{m}\frac{\partial^2 u(x,t)}{\partial t^2} + \bar{c}\frac{\partial u(x,t)}{\partial t} + \bar{k}u(x,t) - EF\frac{\partial^2 u(x,t)}{\partial x^2} = \bar{k}u_g(x,t) + \bar{c}\frac{\partial u_g(x,t)}{\partial t} \tag{32}$$

with boundary conditions

$$\left.\frac{\partial u(x,t)}{\partial x}\right|_{x=0} = \left.\frac{\partial u(x,t)}{\partial x}\right|_{x=l} = 0 \tag{33}$$

and initial conditions

$$u(x,t)|_{t=0} = \left.\frac{\partial u(x,t)}{\partial t}\right|_{t=0} = 0, \tag{34}$$

where $\bar{m}$ is the mass per unit length of the pipe, $\bar{c}$ and $\bar{k}$ the damping and stiffness per unit length of the soil–structure interaction, E and F the modulus of elasticity and cross-sectional area of the pipe, l, the total length of pipeline accounted for, respectively.

4.2. RKPM formulation

Letting $v = \delta u$ be any admissible variation of u, and also introducing Lagrange multipliers to incorporate boundary conditions, the weak form to the strong form given by Eq. (32) with associated boundary conditions Eq. (33) is given as follows:

$$\frac{\bar{m}}{EF}\int_x vu_{,tt}\,\mathrm{d}x + \frac{\bar{c}}{EF}\int_x vu_{,t}\,\mathrm{d}x + \frac{\bar{k}}{EF}\int_x vu\,\mathrm{d}x + \int_x v_{,x}u_{,x}\,\mathrm{d}x - \int_x v\frac{P(x,t)}{EF}\,\mathrm{d}x - 2vu_{,x}\Big|_0^l = 0, \tag{35}$$

where

$$P(x,t) = \bar{k}u_g(x,t) + \bar{c}\frac{\partial u_g(x,t)}{\partial t}.$$

Denoting $\mathbf{u} = \{u_1, u_2, \ldots, u_{NP}\}^{\mathrm{T}}$ the column vector consisting of nodal displacements, the discrete non-linear equations are obtained as follows:

$$\mathbf{M}\mathbf{u}_{,tt} + \mathbf{D}\mathbf{u}_{,t} + \mathbf{R}^{stat}(\mathbf{u}) = \mathbf{0} \tag{36}$$

where $\mathbf{u}_{,t}$ and $\mathbf{u}_{,tt}$ are the first and second derivatives of vector $\mathbf{u}$ with respect to time t, respectively. $\mathbf{M}$ is the mass matrix with its Ath row and Bth column element defined as

$$\mathbf{M}_{AB} = \int_x N_A\left(\frac{\bar{m}}{EF}\right)N_B\,\mathrm{d}x. \tag{37}$$

and $\mathbf{D}$ is the damping matrix with its entries given by

$$\mathbf{D}_{AB} = \int_x N_A\left(\frac{\bar{c}}{EF}\right)N_B\,\mathrm{d}x. \tag{38}$$

$\mathbf{R}^{stat}(\mathbf{u})$ is the static residual and its Ath row element has the form

$$R_A^{Stat}(u) = \frac{\bar{k}}{EF}\int_x N_A\sum_{B=1}^{NP}N_B u_B\,\mathrm{d}x + \int_x N_{A,x}\sum_{B=1}^{NP}N_{B,x}u_B\,\mathrm{d}x - \int_x N_A\frac{P(x,t)}{EF}\,\mathrm{d}x - 2\left(N_A\sum_{B=1}^{NP}N_{B,x}u_B\right)\Big|_0^l. \tag{39}$$

For pseudo-static analysis, only $\mathbf{R}^{stat}(\mathbf{u})$ remains in Eq. (36) and it becomes

$$\mathbf{R}^{stat}(\mathbf{u}) = \mathbf{0}. \tag{40}$$

For dynamic analysis, the displacement at time t_{n+1} can be computed by solving the following system of equations:

$$\mathbf{M}\left(\frac{\mathbf{u}_{n+1}-2\mathbf{u}_n+\mathbf{u}_{n-1}}{\Delta t^2}\right)+\mathbf{D}\left(\frac{\mathbf{u}_{n+1}-\mathbf{u}_n}{\Delta t}\right)+\mathbf{R}^{stat}(\mathbf{u}_{n+1})=\mathbf{0}, \tag{41}$$

where $\mathbf{u}_{n+1}$, $\mathbf{u}_n$ and $\mathbf{u}_{n-1}$ are the displacements at times t_{n+1}, t_n and t_{n-1}, respectively, and Δt is the time step. Eq. (41) can be solved by Newton method, and the ith displacement increment denoted by $\delta\mathbf{u}_{n+1}^{(i)}$ in a Newton approach to compute the displacement $\mathbf{u}_{n+1}$ is given as follows:

$$\left[\frac{\mathbf{M}}{\Delta t^2}+\frac{\mathbf{D}}{\Delta t}+\mathbf{J}(\mathbf{u}_{n+1}^{(i)})\right]\delta\mathbf{u}_{n+1}^{i}=-\left[\mathbf{M}\left(\frac{\mathbf{u}_{n+1}-2\mathbf{u}_n+\mathbf{u}_{n-1}}{\Delta t^2}\right)+\mathbf{D}\left(\frac{\mathbf{u}_{n+1}-\mathbf{u}_n}{\Delta t}\right)+\mathbf{R}^{stat}(\mathbf{u}_{n+1})\right], \tag{42}$$

where the Jacobian matrix $\mathbf{J}$ is defined as

$$\mathbf{J}(\mathbf{u}_{n+1}^{(i)})=\frac{\partial\mathbf{R}^{stat}(\mathbf{u}_{n+1})}{\partial\mathbf{u}_{n+1}} \tag{43}$$

with its Ath row and Bth column element given by

$$\mathbf{J}_{AB}(u)=\frac{\bar{k}}{EF}\int_x N_A N_B\,\mathrm{d}x+\int_x N_{A,x}N_{B,x}\,\mathrm{d}x-2N_A N_{B,x}|_0^l. \tag{44}$$

4.3. RKPM results

Assuming a longitudinal wave travels from left end to the right end of pipe with wave propagation speed c , the acceleration of ground can be given as

$$\frac{\partial^2 u_g(x,t)}{\partial t^2}=\begin{cases}\ddot{u}_0\sin\bar{w}\left(t-\dfrac{x}{c}\right), & \dfrac{x}{c}\leqslant t\leqslant\dfrac{2\pi}{\bar{w}}+\dfrac{x}{c},\\ 0 & \text{otherwise.}\end{cases} \tag{45}$$

The corresponding ground displacement is in the form

$$u_g(x,t)=\begin{cases}\dfrac{\ddot{u}_0}{\bar{w}}\left(t-\dfrac{x}{c}\right)-\dfrac{\ddot{u}_0}{\bar{w}^2}\sin\bar{w}\left(t-\dfrac{x}{c}\right), & \dfrac{x}{c}\leqslant t\leqslant\dfrac{2\pi}{\bar{w}}+\dfrac{x}{c},\\ 0 & \text{otherwise.}\end{cases} \tag{46}$$

In order to compare with the series analytical results given in Ref. [12], the same parameters are used herein, i.e., $\ddot{u}_0=0.3\ \mathrm{m/s^2}$, $\bar{w}=12.56\ \mathrm{rad/s}$, $l=200\ \mathrm{m}$, $\bar{k}=95.2\ \mathrm{MPa}$, $\bar{m}=2072\ \mathrm{kg/m}$, $E=2\times10^5\ \mathrm{MPa}$, $F=9.75\times10^{-2}\ \mathrm{m^2}$, $\bar{c}=1\times10^5\ \mathrm{kg/(s.m)}$.

Figs. 2and 3 show the pseudo-static longitudinal displacements of the points located 40 and 100 m away from the left end of pipeline, respectively. The results correspond to a case of ground wave travelling at speed of 150 m/s, and are obtained by RKPM and the series analytical method proposed in Ref. [12]. For RKPM, total 51 particles are used to compute the longitudinal displacements. It is observed that the static analysis results of RKPM exactly equal the analytical results. Furthermore, dynamic responses of the same points corresponding to wave propagation speed $c=1500\ \mathrm{m/s}$ are also computed by RKPM and compared with the analytical results, and the results are given in Figs. 4 and 5. From Figs. 2–5, we conclude that RKPM is quite suitable for

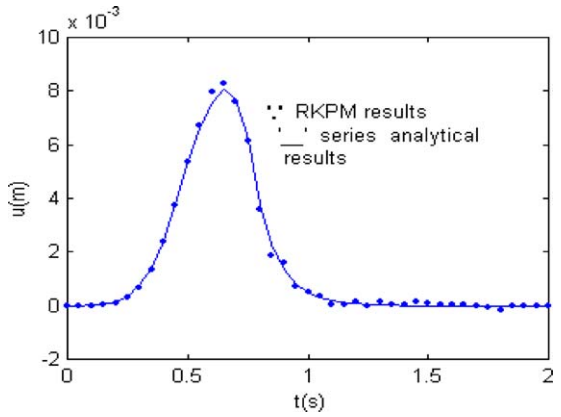

Fig. 2. Static displacement of pipe $x = 40$ m.

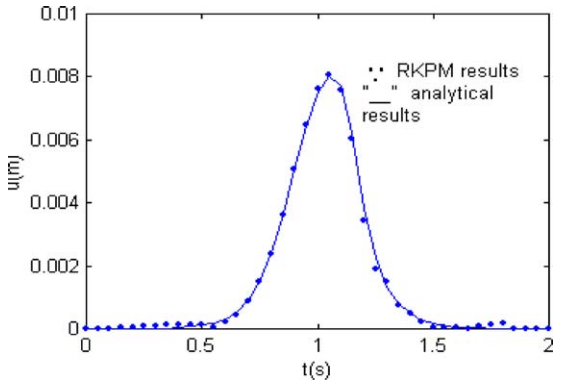

Fig. 3. Static displacement of pipe $x = 100$ m.

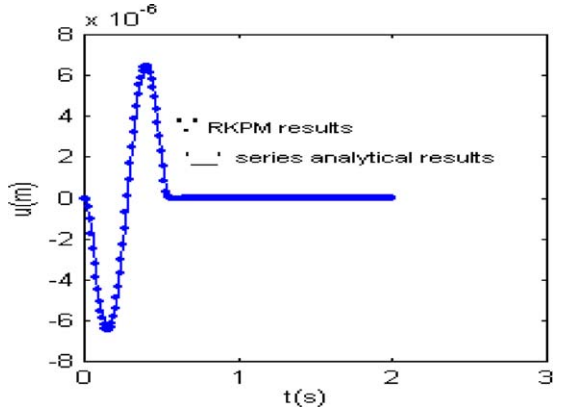

Fig. 4. Dynamic displacement of pipe $x = 40$ m.

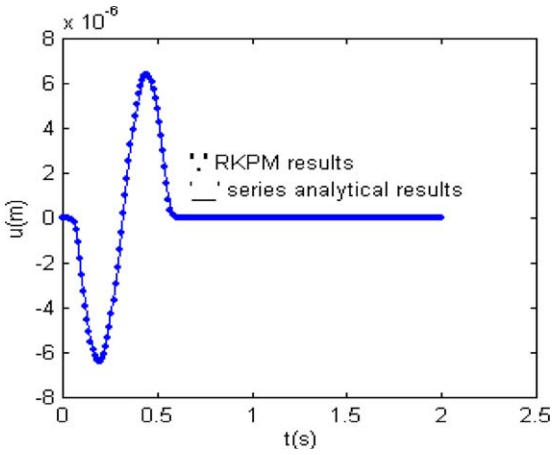

Fig. 5. Dynamic displacement of pipe $x = 100$ m.

Table 4
Comparison between RKPM results and FEM results (unit of displacement: m)

Time (s)	0	0.05	0.1	0.15	0.2	0.25	0.3	0.35	0.4
Analytical	0	1.307E-05	2.492E-04	1.054E-03	2.575E-03	4.688E-03	7.043E-03	9.196E-03	1.078E-02
RKPM	0	1.271E-05	2.481E-04	1.052E-03	2.577E-03	4.697E-03	7.059E-03	9.216E-03	1.080E-02
FEM	0	1.182E-05	2.383E-04	1.018E-04	2.498E-03	4.558E-03	6.858E-03	8.964E-03	1.052E-02

both static and dynamic seismic analysis of buried pipelines. RKPM can, as shown herein, given seismic response of buried pipelines with great accuracy.

In order to test the convergence and effectiveness of RKPM, a comparison is made between the RKPM results and the mesh-based FEM. Only the static displacements of pipeline are computed by both methods with the same number of nodes, i.e., $NP = 21$. The point for calculation is 40 m away from the left end of pipe, and the wave propagates at speed of 1500 m/s. The comparison is given in Table 4. The comparison indicates that RKPM provides a higher rate of convergence than the FEM.

5. Concluding remarks

A meshless approach is presented to accomplish modal analysis of beams and plates as well as to obtain forced vibration response of buried pipelines subjected to longitudinal travelling waves. The meshless approach is based on consistent reproducing kernel approximations, and the domain is discretized by a set of particles without employment of explicit meshes. This paper presents, through introduction of Lagrange multipliers, proper treatment of different boundary conditions and derivation of weak forms of beam free vibration and pipeline forced

vibration. Moreover, alternative transformation method is employed to enforce essential boundary conditions for 2-D plate problems, and RKPM formulation of Kirchhoff plate free vibration problem is also given herein. The numerical results obtained using RKPM method are compared with the results obtained by analytical method or other standard numerical methods such as FEM or Rayleigh–Ritz method. The result of comparison is encouraging regarding free vibration results and force vibration results. Without restriction on simple regular shapes and simple loading conditions, this novel approach has a broader range of application than the analytical method and the Rayleigh–Ritz method. This novel approach, due to no need for explicit mesh and ease for data preparation, also constitutes advantages over the mesh-based FEM method.

Acknowledgements

This research is funded by National Natural Science Foundation of China under Grant Number 10202018. The financial support to the first author is gratefully acknowledged.

References

[1] T. Belytschko, Y. Krongauz, D. Organ, M. Fleming, P. Krysl, Meshless methods: an overview and recent developments, *Computer Methods in Applied Mechanics and Engineering* 139 (1996) 3–47.
[2] W.K. Liu, S. Jun, Y.F. Zhang, Reproducing kernel particle methods, *International Journal for Numerical Methods in Engineering* 20 (1995) 1081–1106.
[3] W.K. Liu, S. Jun, S. Li, J. Adee, T. Belytschko, Reproducing kernel particle methods for structural dynamics, *International Journal for Numerical Methods in Engineering* 38 (1995) 1655–1679.
[4] W.K. Liu, Y. Chen, Wavelet and multiple scale reproducing kernel methods, *International Journal for Numerical Methods in Fluids* 21 (1995) 901–931.
[5] J.S. Chen, C. Pan, C.T. Wu, W.K. Liu, Reproducing kernel particle methods for large deformation analysis of nonlinear structures, *Computer Methods in Applied Mechanics and Engineering* 139 (1996) 195–229.
[6] W.K. Liu, Y. Chen, S. Jun, J.S. Chen, T. Belytschko, C. Pan, R.A. Uras, C.T. Chang, Overview and applications of the reproducing kernel particle methods, *Archives of Computer Methods in Engineering: State of the Art Review* 3 (1996) 3–80.
[7] W.K. Liu, S. Jun, Multiple-scale reproducing kernel particle methods for large deformation problems, *International Journal for Numerical Methods and Engineering* 41 (1998) 1339–1362.
[8] W.K. Liu, S. Jun, S.D. Thomas, Y. Chen, W. Hao, Multiresolution reproducing kernel particle method for computational fluid mechanics, *International Journal for Numerical Methods in Fluids* 24 (1997) 1391–1415.
[9] N.R. Aluru, A reproducing kernel particle method for meshless analysis of microelectromechanical systems, *Computer Mechanics* 23 (1999) 324–338.
[10] A.E. Ouatouati, D.A. Johnson, A new approach for numerical modal analysis using the element-free method, *International Journal for Numerical Methods in Engineering* 46 (1999) 1–27.
[11] G.R. Liu, X.L. Chen, A meshfree method for static and free vibration analysis of thin plates of complicated shape, *Journal of Sound and Vibration* 241 (2001) 839–855.
[12] T.J. Qu, Q.X. Wang, Response of underground pipeline to multi-support longitudinal excitations, *Earthquake Engineering and Engineering Vibration* 13 (1993) 39–45 (in Chinese).